HHS Public Access

Author manuscript

J Control Release. Author manuscript; available in PMC 2017 January 28.

Published in final edited form as:

J Control Release. 2016 January 28; 222: 169–175. doi:10.1016/j.jconrel.2015.12.025.

Magnetically enhanced cell delivery for accelerating recovery of the endothelium in injured arteries

Richard F. Adamo[1], **Ilia Fishbein**[1], **Kehan Zhang**, **Justin Wen**, **Robert J. Levy**, **Ivan S. Alferiev**, and **Michael Chorny**[*]

Department of Pediatrics, The Children's Hospital of Philadelphia, Philadelphia, PA 19104, USA

Abstract

Arterial injury and disruption of the endothelial layer are an inevitable consequence of interventional procedures used for treating obstructive vascular disease. The slow and often incomplete endothelium regrowth after injury is the primary cause of serious short- and long-term complications, including thrombosis, restenosis and neoatherosclerosis. Rapid endothelium restoration has the potential to prevent these sequelae, providing a rationale for developing strategies aimed at accelerating the reendothelialization process. The present studies focused on magnetically guided delivery of endothelial cells (EC) functionalized with biodegradable magnetic nanoparticles (MNP) as an experimental approach for achieving rapid and stable cell homing and expansion in stented arteries. EC laden with polylactide-based MNP exhibited strong magnetic responsiveness, capacity for cryopreservation and rapid expansion, and the ability to disintegrate internalized MNP in both proliferating and contact-inhibited states. Intracellular decomposition of $BODIPY_{558/568}$-labeled MNP monitored non-invasively based on assembly state-dependent changes in the emission spectrum demonstrated cell proliferation rate-dependent kinetics (average disassembly rates: 6.6 ± 0.8% and 3.6 ± 0.4% per day in dividing and contact-inhibited EC, respectively). With magnetic guidance using a transient exposure to a uniform 1-kOe field, stable localization and subsequent propagation of MNP-functionalized EC, markedly enhanced in comparison to non-magnetic delivery conditions, were observed in stented rat carotid arteries. In conclusion, magnetically guided delivery is a promising experimental strategy for accelerating endothelial cell repopulation of stented blood vessels after angioplasty.

Keywords

Arterial injury; Magnetic guidance; Stent angioplasty; Endothelium regrowth; Accelerated reendothelialization; Nanoparticle degradation

1. Introduction

The introduction of intravascular stenting and the more recent redesigning of arterial stents into combination devices providing controlled release of therapeutic agents (namely, drug eluting stents) have dramatically improved therapeutic outcomes of interventional

[*]Corresponding author at: The Children's Hospital of Philadelphia, Abramson Research Building, Suite 702, 3615 Civic Center Boulevard, Philadelphia, PA 19104-4318, USA.chorny@email.chop.edu (M. Chorny).

[1]Contributed equally to this work.

procedures clinically used to relieve obstruction of coronary arteries in vascular disease patients [1]. However, the compression of the endoluminal surface of the blood vessel and extensive trauma inevitably associated with stent implantation together cause extensive endothelial denudation [2,3], and the subsequent recovery of functional endothelium is further markedly delayed by potent antiproliferative drugs released by DES [4]. In absence of an intact endothelial cell layer forming a barrier that modulates local hemostasis and fibrinolysis [5,6], the vulnerability period for late stent thrombosis, a rare but severe complication associated with the use of DES, is markedly prolonged [7,8]. Delayed arterial healing with incomplete endothelialization also contributes to instent neoatherosclerosis, the primary cause of late stent failure [9,10].

Rapid restoration of a continuous and functional endothelial layer is essential for mitigating these untoward effects [6,11]. The recognized therapeutic potential of approaches aimed at accelerating arterial reendothelialization [11] and accessible sources of autologous endothelial cells (EC) [12–14] have prompted exploring endoluminal delivery or direct seeding of EC on vascular stents in experimental settings [15–17]. However, the results of early studies focusing on evaluating these experimental approaches pointed to rapid elimination and low rates of cell engraftment at the injury site [11,14,18] among factors limiting the clinical utility of endothelial cell delivery [19]. The performance of more recently introduced CD34 antibody-coated stents designed to capture endothelial progenitor cells from the blood stream *in situ* has also been shown to be suboptimal, likely due to their insufficient specificity causing recruitment of non-endothelial cells [20–22].

Endowing EC with capacity for physical guidance via functionalization with magnetic nanoparticles (MNP) can potentially be used as part of a targeted delivery strategy effectively confining cells to the stented region and dramatically increasing the rate of endothelial cell repopulation after arterial injury [23,24]. Using biodegradable MNP formulated with strong magnetic responsiveness, such functionalization can be achieved quickly and dose-efficiently through magnetically enhanced endocytosis [25]. In our recent studies, we developed polylactide-based superparamagnetic MNP providing strongly magnetizable EC without compromising cell viability, identified experimental variables controlling the kinetics of magnetically driven cellular uptake, and examined disassembly patterns of the biodegradable MNP using a Förster resonance energy transfer-based approach [25,26]. In the present study, we applied cell functionalization with MNP to investigate feasibility of achieving stable homing and site-specific expansion of syngeneic EC in stented arteries using a two-source magnetic guidance scheme. Unlike single magnetic field sources that fail to provide a sufficiently strong and focused translational force for targeting non-superficial sites in the human body, this targeted delivery approach uses uniform magnetic fields readily achievable in the clinical setting for magnetizing strongly responsive MNP while concomitantly concentrating the magnetic force at the site of stent implantation. The combination of a far-reaching uniform field and strong field gradients induced in the vicinity of the magnetizable implant (secondary source) at the target site makes the two-source strategy potentially scalable for magnetic guidance in human subjects as predicted theoretically [24,27] and more recently confirmed by experimental results in human-sized blood vessels [28,29]. In the context of targeted vascular therapy, this approach

has previously been shown effective by our group at localizing small-molecule drugs, gene delivery vectors and xenogeneic cells in injured arteries [24,30,31]. Herein, we evaluated the efficiency of this magnetic guidance strategy and subsequent fate of stent-targeted EC in a rat carotid stenting model by two complementary methods: direct tissue analysis of cell-associated MNP and quantitative bioluminescent imaging of syngeneic EC stably expressing firefly luciferase as a reporter. Due to its short half-life of ~3 h in mammalian cells [32], stably expressed firefly luciferase serves both as an indicator of the number of viable cells capably of continuously expressing the transgene, and as a marker of their spatial distribution in the region of interest. However, the applicability of the luciferase-based bioluminescent assay for organ distribution analysis is limited by inhomogeneous tissue uptake and highly variable availability of the substrate (luciferin) [33,34]. To address this limitation, an additional approach based on direct fluorimetric analysis of EC functionalized with MNP stably labeled with a boron dipyrromethene fluorophore, $BODIPY_{558/568}$, was applied in this investigation.

2. Materials and methods

2.1. MNP formulation and characterization

$BODIPY_{558/568}$-labeled particle-forming polymer containing 5.7 μmol per g of the covalently bound fluorophore was synthesized as previously described [26] from poly(D,L-lactide) with M_n of 50 kDa (Lakeshore Biomaterials, Birmingham, AL).

Uniformly sized polylactide (PLA)-based magnetic nanoparticles were formulated using a modification of the emulsification-solvent evaporation method [25]. In brief, ethanolic solution of ferric chloride hexahydrate and ferrous chloride tetrahydrate (170 and 62.5 mg, respectively, in 2.5 ml) was added to an equivalent amount of sodium hydroxide dissolved in deionized water (5 ml). The precipitate was maturated for 1 min at 90 °C, cooled on ice and separated on a magnet. The obtained magnetite was stirred with a solution of oleic acid in ethanol (200 mg in 2 ml) at 90 °C for 5 min. Unbound oleic acid was phase-separated with deionized water (4 ml) and removed by decantation. Oleic acid-coated magnetite was washed with ethanol and dispersed in 4 ml of chloroform. $BODIPY_{558/568}$-labeled and plain PLA (80 mg and 120 mg, respectively) were dissolved in 4 ml of chloroform and combined with the chloroformic dispersion of magnetite to form an organic phase. The organic phase was emulsified by sonication on ice in an aqueous solution of bovine serum albumin (2% w/v, 10 ml), and the solvent was removed under reduced pressure using a rotary evaporator. MNP were washed twice by magnetic decantation, resuspended in 6 ml of aqueous trehalose solution (10% w/v), passed through a sterile 5.0 μm polyvinylidene difluoride membrane (EMD Millipore, Billerica, MA) and lyophilized. Lyophilized MNP were kept at −80 °C and resuspended in deionized water before use at 24 mg/ml.

Particle size measurements were performed by dynamic light scattering. Magnetite content was determined spectrophotometrically against a suitable calibration curve (λ = 335 nm) in MNP samples digested for 30 min with sodium hydroxide (1 N) at 37 °C to produce precipitate, which was subsequently dissolved in hydrochloric acid (1 N) by heating to 90 °C for 5 min. Magnetic hysteresis measurements were made using an alternating gradient magnetometer (Princeton Measurements Corporation, Princeton, NJ, USA).

2.2. EC functionalization with MNP and in situ measurements of intracellular MNP disassembly

Rat aortic endothelial cells (EC) from male Lewis rats were purchased from Cell Biologics (Chicago, IL, USA), stably transduced with firefly luciferase under the CMV promoter using Firefly Luciferase Lentifect™ (GeneCopoeia Inc., Rockville, MD, USA) and expanded to passage 4. For MNP functionalization, EC were seeded at 60% of confluence on 96-well plates. On the next day, MNP (3.6 mg) were reconstituted in 0.75 ml rat serum (Bioreclamation, Inc., Westbury, NY, USA) and incubated at 37 °C for 15 min. MNP suspension was diluted 1:50 with serum-free Cell Biologics medium, incubated at 37 °C for an additional 15 min, and added to plated cells at 100 μl per well. The plates were positioned for 24 h on 96-well magnetic separators with an average field gradient of 32.5 T/m (LifeSep 96F, Dexter Magnetic Technologies, Elk Grove Village, IL) to achieve quantitative uptake [25]. The medium was replaced with fresh Cell Biologics medium containing 2% rat serum for 2 h. MNP-laden EC were washed with serum-free culture medium and the amount of internalized MNP was measured fluorimetrically ($\lambda_{em}/\lambda_{ex}$ = 540/575 nm). The iron oxide loading per cell was calculated based on the magnetite content in MNP determined as above. Cells were trypsinized, reconstituted at 2.4×10^5 cells per ml in a freezing medium composed of Pluronic F-68 and dimethyl sulfoxide (1% w/v and 10% v/v, respectively) in rat serum, aliquoted and frozen in Nalgene System 100™ cryogenic tubes (Thermo Fisher Scientific, Rochester, New York, USA) by gradually reducing the temperature to −80 °C at a rate of 1.5 °C/min. For in vitro experiments and animal studies, frozen cells were thawed over 4 min and washed twice with normal saline.

Growth of MNP-functionalized EC seeded on 96-well plates at a density of 2×10^3 cells per well was longitudinally monitored in comparison to non-functionalized EC by luminometry using D-luciferin potassium salt (PerkinElmer, Bridgeville, PA, USA) as a substrate (50 μg/ml), and the obtained results were verified by cell counting. Intracellular disassembly of endocytosed MNP was monitored in EC initially seeded at 2×10^3 and 5×10^4 cells per well based on the ratio of fluorescence intensities at 612 nm and 575 nm (F_{612}/F_{575}) after establishing their correlation in accelerated degradation experiments as previously described [35]. In brief, proteinase K (Sigma-Aldrich, MO, USA) was added at 150 μg/ml to MNP diluted 1:1000 in PBS. Samples were incubated at 37 °C, their emission at λ = 612 and 575 nm were measured at each time point using λ_{ex} = 540 nm, and a part of each sample was passed through an aluminum oxide membrane with a 0.02 μm pore size (Anotop, Whatman Inc., NJ, USA) impermeable to intact particles. Aliquots taken before and after filtration were digested with acetonitrile and analyzed by fluorimetry ($\lambda_{ex}/\lambda_{em}$ = 540 nm/575 nm) to determine the fluorophore fraction enzymatically cleaved off from MNP. The F_{612}/F_{575} ratio of triplicate MNP samples was plotted as a function of the fluorophore fraction dissociated from the particles, and the obtained inverse correlation showing linearity up to 70% of MNP disassembly (Fig. 3C) was applied for determining disintegration of endocytosed MNP by dividing and contact-inhibited EC seeded on 96-well plates.

2.3. In vivo targeting and biodistribution studies

Animal studies were performed in accordance with protocols approved by the Institutional Animal Care and Use Committee of the Children's Hospital of Philadelphia. Under general

anesthesia, the left common carotids of male Lewis rats (350–375 g, n = 10) were isolated through blunt dissection. The external carotids were permanently occluded with a ligature as proximal to the operator as possible, while the internal and common carotids were occluded with a temporary ligature and a vessel clamp, respectively. The left common carotids were injured by 3 passages of a 2F Fogarty embolectomy catheter introduced through an incision made in the left external carotid artery, and a 304-grade stainless steel multilink stent (Laserage Technology Corp., Waukegan, IL, USA) was deployed using an angioplasty balloon catheter (NuMED Inc., Hopkinton, NY, USA). After stent implantation, a 24 gauge 0.5 in. Insyte-N Autogard catheter was inserted into the incision, and the catheter tip advanced until just proximal to the stent. The temporarily isolated segment was filled with 35 μl of a suspension of EC (240 cells per μl) thawed over 4 min and washed in normal saline as above, and a magnetic field of 1 kOe was generated across the area using paired electromagnets positioned at a distance of 40 mm at both sides of the animal. After 1 min, the temporary ligature on the internal carotid and the vessel clamp on the common carotid were released to restore the blood flow, and the magnetic field was maintained for an additional 15 min. The catheter was removed, and the external carotid artery was tied off. Additional animals were treated as above without the exposure to the magnetic field with equivalent doses of MNP-loaded or unloaded EC (n = 9 and 6, respectively). Cell-associated luciferase signal in the stented arteries was imaged and quantified 1 and 7 days post-treatment using an IVIS Spectrum optical imaging system (Caliper Life Sciences, Hopkinton, MA, USA) following a tail vein injection of luciferin potassium salt solution in PBS (25 mg in 500 μl).

In biodistribution studies, MNP-functionalized EC were delivered with or without the magnetic exposure as above (n = 10 and 10, respectively). At 1 and 7 days post treatment, the stented arteries, equally sized segments of the contralateral carotid arteries, and organ tissue samples, including liver, spleen, lung and kidney, were collected from 5 animals in each group, weighed, and homogenized using a bullet blender (Next Advance, Averill Park, NY, USA) for 15 min at 4 °C. Homogenized samples were extracted in two steps with acetonitrile, the organic phase was separated by adding aqueous sodium chloride solution (5 M), and the amounts of the $BODIPY_{558/568}$-labeled polymer were measured in the extracts using λ_{ex} and λ_{em} of 540 nm and 575 nm, respectively.

2.4. Statistical analysis

Cell proliferation and MNP disassembly rates were compared using the single-factor ANOVA. The Kruskal–Wallis non-parametric ANOVA with Dunn's post hoc test were used for *in vivo* data analysis. Differences were termed significant at $p < 0.05$.

3. Results

PLA-based MNP incorporating nanocrystalline magnetite (43% w/w) were produced using a formulation strategy providing uniformly sized particles with an average diameter of 270 ± 10 nm [25]. Magnetically enhanced MNP uptake and EC functionalization resulted in a MNP loading corresponding to 29.8 ± 0.1 pg iron oxide/cell, with MNP exhibiting perinuclear distribution in the cell interior characteristic of endocytosed particles (Fig. 1A). Consistent with magnetic properties of the MNP formulation (Fig. 1B), functionalized cells

showed strong yet fully reversible magnetization, with 60% of the saturation value (980 pemu/cell, Fig. 1C) reached at 1 kOe, the field intensity employed for stent-targeted delivery in the present studies. Notably, the magnetic remanence of MNP-laden EC amounted to less than 1% of the magnetic moment measured at 1 kOe, suggesting that functionalized cells will only exhibit magnetization in the field presence. In contrast, unloaded EC were diamagnetic, showing weak repulsion when exposed to a magnetizing field (Fig. 1C).

Cryopreservation without compromising cell viability is a critical aspect of the clinical translation and implementation of cell therapeutics [36,37]. However, despite extensive research on optimizing cryopreservation techniques, achieving adequate recovery of cryopreserved cells has been challenging [38]. MNP-laden EC cryopreserved in a medium supplemented with Pluronic F-68, an effective plasma membrane “sealant” shown to promote cellular wound healing [39–41], consistently exhibited ≥90% post-thaw recovery, unaltered morphology, and capacity for substrate attachment comparable to those of unloaded cells in the present study (Fig. 2). Rapid expansion of functionalized cells, a prerequisite for accelerated endothelium regrowth, was accompanied by MNP payload dilution with internalized particles distributed between daughter cells and occurred at a rate equal to that of unloaded cells as evidenced by microscopic observations (Fig. 2D, F) and determined quantitatively by bioluminescence showing cell propagation 14 ± 1 and 27 ± 1 times by days 6 and 8 post seeding, respectively (Fig. 2G).

Intracellular disassembly of MNP was studied using an approach taking advantage of dynamic changes in the fluorescence spectrum of particles covalently labeled with a boron dipyrromethene fluorophore, $BODIPY_{558/568}$, as a function of their integrity status. In addition to an emission maximum at 575 nm characteristic of this probe [42], the spectrum of $BODIPY_{558/568}$-labeled intact MNP excited at λ_{ex} = 540 nm also features a prominent peak at 612 nm [26,35]. This peak in turn reaches its maximal intensity when MNP are excited at λ_{ex} = 565 nm (Fig. 3A, B). This feature of the MNP fluorescence pattern suggests the formation of a complex, likely a dimer of the polymer-conjugated $BODIPY_{558/568}$, exhibiting red-shifted excitation and emission and engaging in energy transfer with the monomeric probe enabled by an extensive overlap in their spectra. Disintegration of these complexes in the process of particle disassembly results in disruption of the energy transfer and can be reliably monitored by measuring the ratio of fluorescence intensities at 612 nm and 575 nm (F_{612}/F_{575}). In accelerated degradation studies, F_{612}/F_{575} decreased linearly from 0.77 (intact particles) to 0.37 (MNP disintegrated by 70%, Fig. 3C). The distinct disassembly profiles observed using this analytical approach for endocytosed MNP in dividing vs. contact-inhibited EC point to a significant effect of cell proliferation on the MNP intracellular processing kinetics ($p = 0.002$, Fig. 3D). Over 5 days, endocytosed MNP disintegrated by 34 ± 4% in the interior of dividing EC (average disassembly rate of 6.6 ± 0.8% per day). In comparison, with disassembly progressing at an average rate of 3.6 ± 0.4% per day, the extent of MNP disintegration in quiescent cells was 19 ± 1% by this time point.

Magnetically guided delivery of MNP-functionalized EC to stented arteries and their expansion at the site of stent deployment were studied by bioluminescent imaging in the rat carotid model of stent angioplasty. Unmodified or MNP-laden EC delivered under non-

magnetic conditions were included as controls. With magnetic guidance, enhanced localization of luciferase-expressing EC to the stented region was observed at both 1 and 7 days post treatment in comparison to the control groups ($p < 0.018$, Fig. 4). The cell-associated bioluminescent signal measured in the arteries of magnetically treated animals was spatially confined to the stented segment (Fig. 4A, D) and notably increased between the two time points, indicating that EC underwent a marked expansion in the stented region over 7 days after their magnetically guided delivery (Fig. 4G).

Fluorescently labeled MNP were employed as an additional marker of functionalized EC allowing their quantitative analysis in harvested tissues using a fluorimetric assay of the particle-forming polymer. Interestingly, while fluorimetric assay results confirmed the superior site-specificity of cell delivery achievable with magnetic guidance, they also revealed a notably higher ratio of the marker signal between the magnetic and non-magnetic (control) groups in comparison to quantitative bioluminescent imaging data at 1 day post treatment (Fig. 5A vs. Fig. 4G). A similar difference between the results of bioluminescent imaging and direct tissue analysis was previously observed by our group [31], and may be attributed to obscuration of a portion of the luciferase-derived light blocked by the opaque stent struts in the former technique. Based on the MNP assay data and the previously established MNP loading per cell, the calculated number of MNP-functionalized EC delivered to the stented arteries with magnetic guidance was 3020 ± 1100, corresponding to 36% of the administered dose. In contrast, a MNP amount equivalent to 60 ± 30 cells (i.e. 0.7% of the applied cell dose) was found in the stented arteries of the non-magnetically treated animals (Fig. 5A, $p = 0.004$ vs. magnetic delivery). Notably, in contrast to the bioluminescent signal substantially increasing with the number of viable cells in the stented region between days 1 and 7 in magnetically treated animals, the amount of cell-associated MNP determined in the stented arteries decreased over the same time period from 20.7 ± 6.3 to 5.9 ± 1.4 ng/mg (Fig. 5A, B), likely as a result of several concomitant processes that included particle disassembly and subsequent elimination of the particle-forming components. Tissue weight-normalized amounts of MNP detected in the peripheral tissues of magnetically and non-magnetically treated animals, including contralateral arteries, liver, spleen, lungs and kidneys, were less than 1.3 ng/mg at both time points.

4. Discussion

Increased susceptibility to thrombosis and restenosis due to slow and often incomplete regrowth of the endothelial layer severely damaged as a result of extensive mechanical injury remains a critical limitation of interventional strategies currently used clinically to relieve atherosclerotic obstruction [43,44]. Rapid endothelium recovery and restoration of its normal functions have the potential to both prevent the thrombotic events and limit post-angioplasty restenosis [2,5,45], providing the rationale for developing strategies aimed at accelerating arterial reendothelialization. In the present study, we investigated functionalization of EC with biodegradable MNP and feasibility of achieving with magnetically guided delivery their stable homing, expansion and sustained presence in stented arteries.

For effectively using magnetically guided cell delivery to promote endothelium recovery, the ability to provide cells with sufficient magnetic responsiveness without adversely affecting their viability and proliferation capacity is essential. Nanoparticle loading and cell cryopreservation required for completion of safety and quality control testing, transportation and subsequent use, all parts of the “manufacturability” of a cell therapy product [36,37], can expose cells to different types of stress and affect the recovery yield of the cell preparation process. We previously demonstrated that superparamagnetic polylactide-based MNP coated with albumin could be used for rapid and dose-efficient production of magnetically responsive EC without significantly compromising their viability and capacity for substrate attachment [25]. As part of these studies, optimal cell functionalization conditions and a threshold of MNP loading providing individual cells with responsiveness sufficient for their effective magnetic guidance were identified. Others have also shown that internalization of similarly designed MNP does not markedly affect cytoskeleton integrity and cell respiration of EC [46]. In the present study we established feasibility of cryopreserving MNP-laden EC using a membrane sealing agent of the polyalkylene glycol family, Pluronic F-68. Freeze-thawing procedures can cause cell membrane injury due to ice nucleation and the damaging effects of increasing salt concentration [47], which in turn can compromise cell survival and significantly delay growth of the remaining cells after thawing [39]. Pluronic F-68 has previously been shown to promote cellular wound healing [40] and minimize cryodamage when included in the freezing medium [41]. In contrast to standard freezing media, no lag in the proliferation onset after thawing was observed when Pluronic F-68 was used at concentrations between 0.1 to 5%, with a notable increase in cell number observed already in the first 24 h [39]. Our results show that MNP-functionalized EC cryopreserved in a medium containing 1% Pluronic F-68 exhibit excellent recovery and high proliferation capacity with 5 population doublings over 8 days post thawing (Fig. 2). These *in vitro* findings were paralleled by survival of stent-targeted cells and their rapid expansion demonstrated *in vivo* in rat carotid stenting model experiments, where a marked increase in the bioluminescent signal associated with magnetically guided cells was evident between days 1 and 7 post treatment.

Stent-targeted delivery poses a set of requirements with regard to the durability and pattern of the magnetic responsiveness of functionalized cells. A strong magnetic moment in response to an externally applied uniform field is needed over a defined time period to enable guidance and stable cell attachment in the target region. In this study, a brief exposure to a field of 1 kOe magnetizing cells strongly yet fully reversibly was shown to be sufficient to allow their anchorage and retention in the stented arterial segment in the presence of blood flow. Importantly, the reversible character of cell magnetization imparted by the particles designed with superparamagnetic properties makes possible “turning off” the magnetic interactions after stent-targeted delivery, thus obviating the risk of magnetically induced, irreversible clumping and capillary blockage by cells failing to attach stably to the target site before the completion of the delivery phase.

Bioeliminability of MNP used for cell functionalization is another important determinant of the general safety of magnetically guided cell delivery. Decomposition of the polyester-based particle matrix controllable through adjustments in the molecular weight and

composition of the particle-forming polymer allows MNP to disintegrate in the cell interior as shown in the present study using a simple approach based on monitoring assembly state-dependent changes in the emission spectrum of $BODIPY_{558/568}$-labeled particles. Both proliferating and quiescent EC were able to decompose the internalized particle payload in agreement with the results of our previous study where disassembly rates of endocytosed MNP were examined in vascular cells using global Förster resonance energy transfer analysis [26]. However, the faster processing kinetics, possibly due to an increasing contribution of "biotic", presumably enzyme-mediated, mechanisms activated in dividing cells, suggest that particle disintegration and elimination from stent-targeted EC are likely to be most rapid during the phase of active cell division, and will proceed at a slower rate as more cells become contact-inhibited [26]. The ability of stent-targeted EC to decompose and eliminate MNP *in vivo* is supported by a notable reduction in the amount of cell-associated MNP in stented arteries in the period between 1 and 7 days after treatment. However, the disappearance of MNP from the region of stent placement occurred at a markedly faster overall rate compared to MNP disassembly in cultured EC, suggesting that the *in vivo* process is more complex, possibly involving regulation by additional factors or including other mechanisms contributing to the elimination of MNP used for EC functionalization. The subsequent processing and eventual removal of the products formed by MNP disassembly (lactide oligomers and lactic acid, albumin and its fragments, iron oxide) is expected to occur on different respective time-scales through distinct metabolic pathways [48–50].

Previous studies in rat and rabbit models of arterial injury have shown that endothelial regrowth proceeds slowly from the margins of the denuded area and can halt after several weeks, even though large zones of the vessel may still be devoid of endothelium [3,51]. The rate and pattern of this process can, however, be shifted to provide faster cell repopulation and more complete coverage by positioning additional sources of endothelial outgrowth within the denuded region [52]. In the magnetic guidance approach evaluated in the present study, the magnetic force is applied to generate such foci of endothelial outgrowth along the stented arterial segment. Notably, after the initial 1-min occlusion of the targeted arterial segment, the magnetic exposure was continued for an additional 15 min in the presence of the restored blood flow, as an experimental model of a more clinically practical scenario. Our results demonstrate that the high-gradient magnetic field induced in the vicinity of the stent struts over this limited time period was effective at allowing MNP-functionalized EC withstand the hemodynamic force exerted by the blood flow and promoted cell attachment to the site of stent deployment *in vivo*. This observation is in agreement with rapid magnetically driven substrate attachment of MNP-functionalized EC challenged with an opposing force that was previously demonstrated *in vitro* by our group [25].

5. Conclusions

The slow cell repopulation from the margins of the injured area delays restoration of the endothelial barrier normally protecting blood vessels against thrombosis and inflammation. The present study examined the feasibility of guided cell delivery via a transient exposure to a uniform magnetizing field to enhance capture, retention and proliferation of EC at the site of stent implantation as a means to accelerate the endothelial cell repopulation process. Our

findings central to the goal of accelerating recovery of denuded endothelium in stented blood vessels include the high site-specificity of the two-source magnetic cell guidance and the stable anchorage and marked propagation of targeted syngeneic EC at the site of stent deployment. Using bioluminescent imaging and fluorimetric tissue analysis as two complementary approaches for studying the fate of stent-targeted EC and cell-associated MNP, we have shown that 1) magnetically guided cells will home and expand at the site of stent implantation, 2) targeted cell delivery realized with a brief exposure to a magnetizing field of a clinically applicable strength can dramatically improve site specificity as evidenced by the target:nontarget ratio markedly increased in comparison to non-magnetically treated control animals, 3) in agreement with the results of *in vitro* experiments, elimination of MNP used for EC functionalization will take place concomitantly with cell expansion after the completion of the targeted delivery step. The present study contributes to establishing effectiveness and safety of magnetically guided cell delivery and shows the potential of this approach for accelerating the healing of injured blood vessels and reducing vulnerability to untoward effects associated with stent implantation.

Acknowledgments

The authors thank Gary Friedman (Drexel University, Philadelphia, PA, USA) for advising on the magnetic delivery strategy, and NuMED, Inc. (Hopkinton, NY, USA) for providing rat angioplasty catheters. This research was supported by the U.S. National Heart, Lung, and Blood Institute grant R01-HL111118 (MC), and The Children's Hospital of Philadelphia Research Funds including the William J. Rashkind Endowment, Erin's Fund, and The Kibel Foundation (RJL).

References

1. Coolong A, Kuntz RE. Understanding the drug-eluting stent trials. Am J Cardiol. 2007; 100(5A): 17K–24K.
2. Douglas G, Van Kampen E, Hale AB, McNeill E, Patel J, Crabtree MJ, Ali Z, Hoerr RA, Alp NJ, Channon KM. Endothelial cell repopulation after stenting determines in-stent neointima formation: effects of bare-metal vs. drug-eluting stents and genetic endothelial cell modification. Eur Heart J. 2012; 34(43):3378–3388. [PubMed: 23008511]
3. Stemerman MB, Spaet TH, Pitlick F, Cintron J, Lejnieks I, Tiell ML. Intimal healing. The pattern of reendothelialization and intimal thickening. Am J Pathol. 1977; 87(1):125–142. [PubMed: 322503]
4. Nakazawa G, Finn AV, Virmani R. Vascular pathology of drug-eluting stents. Herz. 2007; 32(4): 274–280. [PubMed: 17607533]
5. Fuchs AT, Kuehnl A, Pelisek J, Rolland PH, Mekkaoui C, Netz H, Nikol S. Inhibition of restenosis formation without compromising reendothelialization as a potential solution to thrombosis following angioplasty? Endothelium. 2008; 15(1):85–92. [PubMed: 18568948]
6. Otsuka F, Finn AV, Yazdani SK, Nakano M, Kolodgie FD, Virmani R. The importance of the endothelium in atherothrombosis and coronary stenting. Nat Rev Cardiol. 2012; 9(8):439–453. [PubMed: 22614618]
7. Harper RW. Drug-eluting coronary stents—a note of caution. Med J Aust. 2007; 186(5):253–255. [PubMed: 17391089]
8. Iakovou I, Schmidt T, Bonizzoni E, Ge L, Sangiorgi GM, Stankovic G, Airoldi F, Chieffo A, Montorfano M, Carlino M, Michev I, Corvaja N, Briguori C, Gerckens U, Grube E, Colombo A. Incidence, predictors, and outcome of thrombosis after successful implantation of drug-eluting stents. JAMA. 2005; 293(17):2126–2130. [PubMed: 15870416]
9. Park SJ, Kang SJ, Virmani R, Nakano M, Ueda Y. In-stent neoatherosclerosis: a final common pathway of late stent failure. J Am Coll Cardiol. 2012; 59(23):2051–2057. [PubMed: 22651862]

10. Nakazawa G, Otsuka F, Nakano M, Vorpahl M, Yazdani SK, Ladich E, Kolodgie FD, Finn AV, Virmani R. The pathology of neoatherosclerosis in human coronary implants bare-metal and drug-eluting stents. J Am Coll Cardiol. 2011; 57(11):1314–1322. [PubMed: 21376502]
11. Versari D, Lerman LO, Lerman A. The importance of reendothelialization after arterial injury. Curr Pharm Des. 2007; 13(17):1811–1824. [PubMed: 17584110]
12. Froehlich H, Gulati R, Boilson B, Witt T, Harbuzariu A, Kleppe L, Dietz AB, Lerman A, Simari RD. Carotid repair using autologous adipose-derived endothelial cells. Stroke. 2009; 40(5):1886–1891. [PubMed: 19286583]
13. Han JK, Chang SH, Cho HJ, Choi SB, Ahn HS, Lee J, Jeong H, Youn SW, Lee HJ, Kwon YW, Oh BH, Oettgen P, Park YB, Kim HS. Direct conversion of adult skin fibroblasts to endothelial cells by defined factors. Circulation. 2014; 130(14):1168–1178. [PubMed: 25186941]
14. Gulati R, Jevremovic D, Witt TA, Kleppe LS, Vile RG, Lerman A, Simari RD. Modulation of the vascular response to injury by autologous blood-derived outgrowth endothelial cells. Am J Physiol Heart Circ Physiol. 2004; 287(2):H512–H517. [PubMed: 15072951]
15. van der Giessen WJ, Serruys PW, Visser WJ, Verdouw PD, van Schalkwijk WP, Jongkind JF. Endothelialization of intravascular stents. J Interv Cardiol. 1988; 1(2):109–120.
16. Gulati R, Lerman A, Simari RD. Therapeutic uses of autologous endothelial cells for vascular disease. Clin Sci (Lond). 2005; 109(1):27–37. [PubMed: 15966869]
17. Parikh SA, Edelman ER. Endothelial cell delivery for cardiovascular therapy. Adv Drug Deliv Rev. 2000; 42(1–2):139–161. [PubMed: 10942819]
18. Griese DP, Ehsan A, Melo LG, Kong D, Zhang L, Mann MJ, Pratt RE, Mulligan RC, Dzau VJ. Isolation and transplantation of autologous circulating endothelial cells into denuded vessels and prosthetic grafts: implications for cell-based vascular therapy. Circulation. 2003; 108(21):2710–2715. [PubMed: 14597586]
19. Dimmeler S, Leri A. Aging and disease as modifiers of efficacy of cell therapy. Circ Res. 2008; 102(11):1319–1330. [PubMed: 18535269]
20. Garg S, Duckers HJ, Serruys PW. Endothelial progenitor cell capture stents: will this technology find its niche in contemporary practice? Eur Heart J. 2010; 31(9):1032–1035. [PubMed: 20064819]
21. Szmitko PE, Kutryk MJ, Stewart DJ, Strauss MH, Verma S. Endothelial progenitor cell-coated stents under scrutiny. Can J Cardiol. 2006; 22(13):1117–1119. [PubMed: 17102828]
22. Wendel HP, Avci-Adali M, Ziemer G. Endothelial progenitor cell capture stents —hype or hope? Int J Cardiol. 2009; 145(1):115–117. [PubMed: 19576642]
23. Pislaru SV, Harbuzariu A, Gulati R, Witt T, Sandhu NP, Simari RD, Sandhu GS. Magnetically targeted endothelial cell localization in stented vessels. J Am Coll Cardiol. 2006; 48(9):1839–1845. [PubMed: 17084259]
24. Polyak B, Fishbein I, Chorny M, Alferiev I, Williams D, Yellen B, Friedman G, Levy RJ. High field gradient targeting of magnetic nanoparticle-loaded endothelial cells to the surfaces of steel stents. Proc Natl Acad Sci U S A. 2008; 105(2):698–703. [PubMed: 18182491]
25. Chorny M, Alferiev IS, Fishbein I, Tengood JE, Folchman-Wagner Z, Forbes SP, Levy RJ. Formulation and in vitro characterization of composite biodegradable magnetic nanoparticles for magnetically guided cell delivery. Pharm Res. 2012; 29(5):1232–1241. [PubMed: 22274555]
26. Tengood JE, Alferiev IS, Zhang K, Fishbein I, Levy RJ, Chorny M. Real-time analysis of composite magnetic nanoparticle disassembly in vascular cells and biomimetic media. Proc Natl Acad Sci U S A. 2014; 111(11):4245–4250. [PubMed: 24591603]
27. Yellen BB, Forbes ZG, Halverson DS, Fridman G, Barbee KA, Chorny M, Levy R, Friedman G. Targeted drug delivery to magnetic implants for therapeutic applications. J Magn Magn Mater. 2005; 293:647–654.
28. Kempe H, Kates SA, Kempe M. Nanomedicine's promising therapy: magnetic drug targeting. Expert Rev Med Devices. 2011; 8(3):291–294. [PubMed: 21542699]
29. Kempe H, Kempe M, Snowball I, Wallen R, Arza CR, Gotberg M, Olsson T. The use of magnetite nanoparticles for implant-assisted magnetic drug targeting in thrombolytic therapy. Biomaterials. 2010; 31(36):9499–9510. [PubMed: 20732712]

30. Chorny M, Fishbein I, Yellen BB, Alferiev IS, Bakay M, Ganta S, Adamo R, Amiji M, Friedman G, Levy RJ. Targeting stents with local delivery of paclitaxel-loaded magnetic nanoparticles using uniform fields. Proc Natl Acad Sci U S A. 2010; 107(18):8346–8351. [PubMed: 20404175]
31. Chorny M, Fishbein I, Tengood JE, Adamo RF, Alferiev IS, Levy RJ. Site-specific gene delivery to stented arteries using magnetically guided zinc oleate-based nano-particles loaded with adenoviral vectors. FASEB J. 2013; 27(6):2198–2206. [PubMed: 23407712]
32. Thompson JF, Hayes LS, Lloyd DB. Modulation of firefly luciferase stability and impact on studies of gene regulation. Gene. 1991; 103(2):171–177. [PubMed: 1889744]
33. Berger F, Paulmurugan R, Bhaumik S, Gambhir SS. Uptake kinetics and biodistribution of 14C-D-luciferin—a radiolabeled substrate for the firefly luciferase catalyzed bioluminescence reaction: impact on bioluminescence based reporter gene imaging. Eur J Nucl Med Mol Imaging. 2008; 35(12):2275–2285. [PubMed: 18661130]
34. Lee KH, Byun SS, Paik JY, Lee SY, Song SH, Choe YS, Kim BT. Cell uptake and tissue distribution of radioiodine labelled D-luciferin: implications for luciferase based gene imaging. Nucl Med Commun. 2003; 24(9):1003–1009. [PubMed: 12960600]
35. Alferiev IS, Iyer R, Croucher JL, Adamo RF, Zhang K, Mangino JL, Kolla V, Fishbein I, Brodeur GM, Levy RJ, Chorny M. Nanoparticle-mediated delivery of a rapidly activatable prodrug of SN-38 for neuroblastoma therapy. Biomaterials. 2015; 51:22–29. [PubMed: 25770994]
36. Hubel A. Advancing the preservation of cellular therapy products. Transfusion. 2011; 51(Suppl 4): 82S–86S. [PubMed: 22074631]
37. Eaker S, Armant M, Brandwein H, Burger S, Campbell A, Carpenito C, Clarke D, Fong T, Karnieli O, Niss K, Van't Hof W, Wagey R. Concise review: guidance in developing commercializable autologous/patient-specific cell therapy manufacturing. Stem Cells Transl Med. 2013; 2(11):871–883. [PubMed: 24101671]
38. Karlsson JO, Toner M. Long-term storage of tissues by cryopreservation: critical issues. Biomaterials. 1996; 17(3):243–256. [PubMed: 8745321]
39. González Hernández Y, Fischer RW. Serum-free culturing of mammalian cells —adaptation to and cryopreservation in fully defined media. ALTEX. 2007; 24(2):110–116. [PubMed: 17728976]
40. Lee RC. Cytoprotection by stabilization of cell membranes. Ann N Y Acad Sci. 2002; 961:271–275. [PubMed: 12081916]
41. Ashwood-Smith MJ, Voss WA, Warby C. Cryoprotection of mammalian cells in tissue culture with pluronic polyols. Cryobiology. 1973; 10(6):502–504. [PubMed: 4772975]
42. Ma G, Müller AM, Bardeen CJ, Cheng Q. Self-assembly combined with photopolymerization for the fabrication of fluorescence "turn-on" vesicle sensors with reversible "on–off" switching properties. Adv Mater. 2005; 18:55–60.
43. Van Belle E, Bauters C, Asahara T, Isner JM. Endothelial regrowth after arterial injury: from vascular repair to therapeutics. Cardiovasc Res. 1998; 38(1):54–68. [PubMed: 9683907]
44. Guagliumi G, Sirbu V, Musumeci G, Gerber R, Biondi-Zoccai G, Ikejima H, Ladich E, Lortkipanidze N, Matiashvili A, Valsecchi O, Virmani R, Stone GW. Examination of the in vivo mechanisms of late drug-eluting stent thrombosis: findings from optical coherence tomography and intravascular ultrasound imaging. JACC Cardiovasc Interv. 2012; 5(1):12–20. [PubMed: 22230145]
45. Tahir H, Bona-Casas C, Hoekstra AG. Modelling the effect of a functional endothelium on the development of in-stent restenosis. PLoS One. 2013; 8(6):e66138. [PubMed: 23785479]
46. Orynbayeva Z, Sensenig R, Polyak B. Metabolic and structural integrity of magnetic nanoparticle-loaded primary endothelial cells for targeted cell therapy. Nanomedicine (London). 2015; 10(10): 1555–1568.
47. Karlsson JO, Cravalho EG, Borel Rinkes IH, Tompkins RG, Yarmush ML, Toner M. Nucleation and growth of ice crystals inside cultured hepatocytes during freezing in the presence of dimethyl sulfoxide. Biophys J. 1993; 65(6):2524–2536. [PubMed: 8312489]
48. Weissleder R, Stark DD, Engelstad BL, Bacon BR, Compton CC, White DL, Jacobs P, Lewis J. Superparamagnetic iron oxide: pharmacokinetics and toxicity. AJR Am J Roentgenol. 1989; 152(1):167–173. [PubMed: 2783272]

49. Wu XS, Wang N. Synthesis, characterization, biodegradation, and drug delivery application of biodegradable lactic/glycolic acid polymers. Part II: biodegradation. J Biomater Sci Polym Ed. 2001; 12(1):21–34. [PubMed: 11334187]

50. Rothschild MA, Oratz M, Schreiber SS. Albumin metabolism. Gastroenterology. 1973; 64(2):324–337. [PubMed: 4568596]

51. Reidy MA, Clowes AW, Schwartz SM. Endothelial regeneration. V. Inhibition of endothelial regrowth in arteries of rat and rabbit. Lab Investig. 1983; 49(5):569–575. [PubMed: 6632774]

52. Kipshidze N, Dangas G, Tsapenko M, Moses J, Leon MB, Kutryk M, Serruys P. Role of the endothelium in modulating neointimal formation: vasculoprotective approaches to attenuate restenosis after percutaneous coronary interventions. J Am Coll Cardiol. 2004; 44(4):733–739. [PubMed: 15312851]

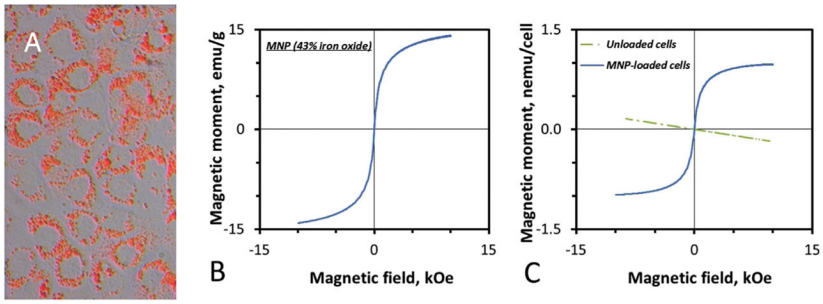

Fig. 1.

Endothelial cells functionalized with polylactide-based MNP. Intracellular localization of MNP internalized by rat aortic endothelial cells over 24 h in presence of a high-gradient field (32.5 T/m) is visualized by fluorescent microscopy using particles stably labeled with $BODIPY_{558/568}$ (merged bright field and red fluorescent image shown in A, original magnification ×400). Polylactide-based MNP formulated with 43% magnetite (w/w) exhibit strong magnetization at 1 kOe (uniform field strength used for *in vivo* studies) and a lack of remanence (B). Consistent with the particle magnetization pattern, MNP-functionalized cells show strong yet fully reversible magnetization (0.6 nemu per cell at 1 kOe) absent in control (unloaded) cells (C).

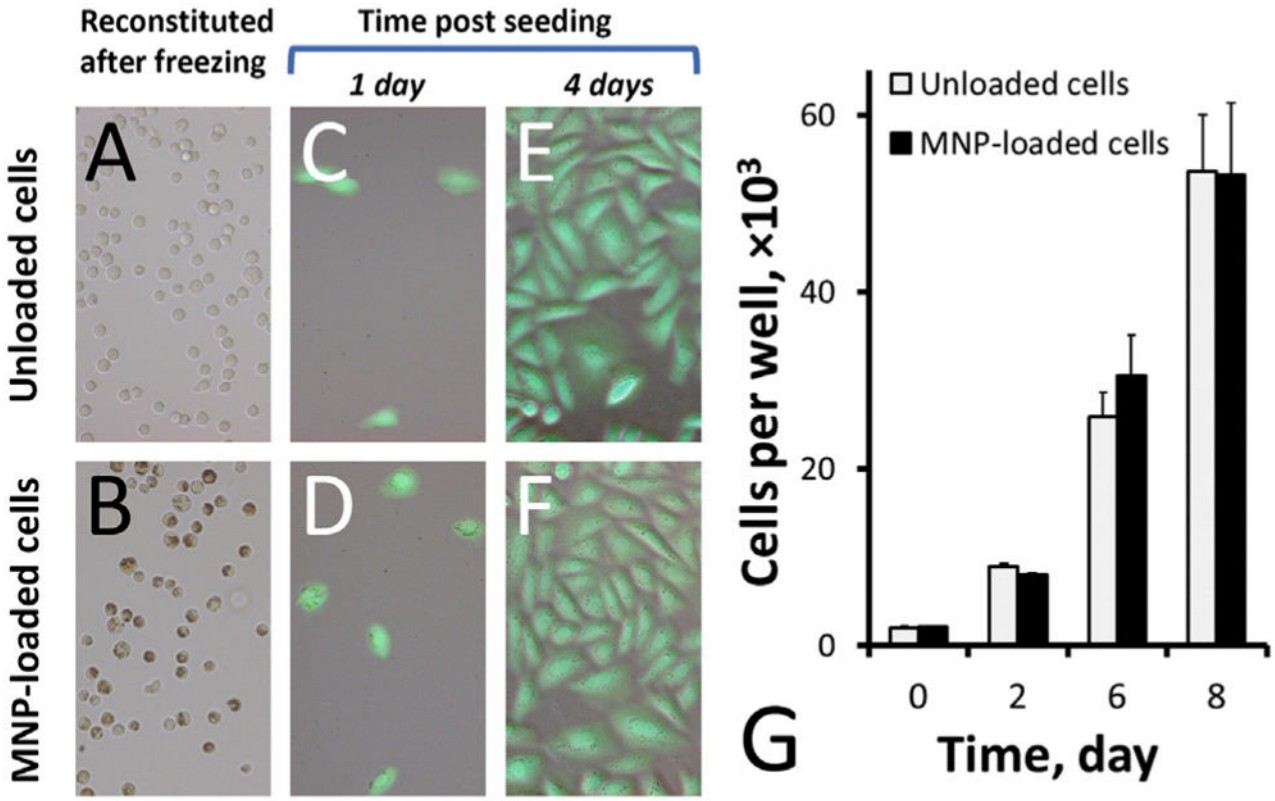

Fig. 2.

Recovery and *in vitro* proliferation of endothelial cells after MNP loading and cryopreservation. Untreated and MNP-functionalized rat aortic endothelial cells frozen in a Pluronic F-68 supplemented cryoprotection medium were thawed over 4 min, washed twice with normal saline and examined microscopically (A and B, respectively). After thawing and seeding on 96-well plates at 2×10^3 cells per well, control and functionalized cells underwent rapid expansion at a comparable rate, as observed by microscopy after staining with a green fluorescent cell viability marker, Calcein AM, at 1 and 4 days post seeding (merged bright field and green fluorescent images shown in C and E vs. D and F, for control and functionalized cells, respectively), and determined quantitatively over 8 days based on the luciferase activity of stably transduced cells (G). Note the presence of MNP in functionalized cells discernible both immediately after thawing and at 1 day post seeding (B and D, respectively). The original magnification in A–F is ×200. Data in G are presented as mean ± SD.

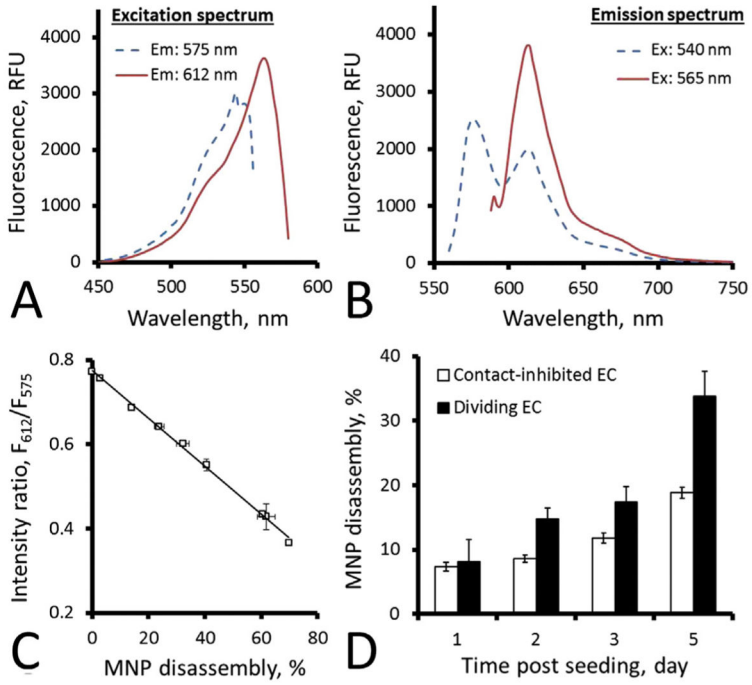

Fig. 3.

In vitro disassembly analysis of MNP in the interior of contact-inhibited and dividing endothelial cells. MNP stably labeled with $BODIPY_{558/568}$ exhibit complex excitation and emission patterns (A and B, respectively) suggesting partial aggregation of the fluorophore to form a species with red-shifted emission ($\lambda = 612$ nm) in intact MNP. Forced degradation of MNP with Proteinase K results in a readily quantifiable decrease in the ratio of fluorescence intensities at $\lambda = 612$ and 575 nm (C). This phenomenon was used for examining directly and non-invasively disassembly rates of polylactide-based MNP in the interior of contact-inhibited and dividing endothelial cells (D). Data in C and D are presented as mean ± SD.

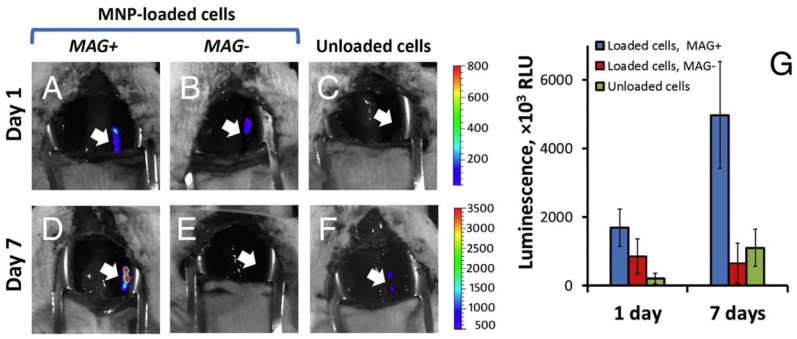

Fig. 4.

Localization and expansion of endothelial cells magnetically guided to stented rat carotid arteries via a transient exposure to a uniform magnetizing field (1 kOe, 15 min). MNP-functionalized rat aortic endothelial cells were administered over 1 min under magnetic conditions to arterial segments implanted with 304-grade stainless steel stents, and the magnetic field was maintained for an additional 15 min after restoring blood flow. Cell-associated luciferase signal in stented arteries was visualized and quantified by live animal bioluminescent imaging at 1 and 7 days post treatment (A and D, respectively) in comparison to non-magnetic delivery of MNP-loaded and unloaded cells (B and E, and C and F, respectively). Arrows indicate stent implantation sites. Quantitative results are shown in G as mean ± SE.

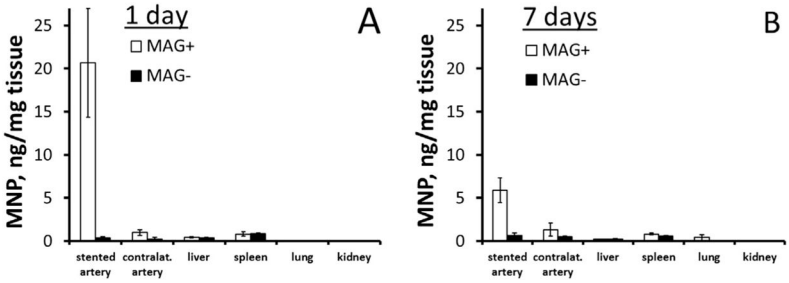

Fig. 5.

Tissue distribution analysis of biodegradable MNP employed for cell functionalization. Tissue weight-normalized amounts of MNP were determined fluorimetrically in homogenized arteries and peripheral tissue samples harvested after 1 and 7 days (A and B, respectively) from animals treated under magnetic vs. non-magnetic conditions. Data are presented as mean ± SE.